Journal of Stress Analysis
Vol. 6, No. 1, Spring – Summer 2021, 89-103

Bu-Ali Sina University

ORIGINAL RESEARCH PAPER

# Transient Coupled Hygrothermal Stress Analysis of a Finite Length Functionally Graded Hollow Cylinder

**M. Saadatfar***
Mechanical Engineering Department, University of Qom, Qom, Iran.

## Article info

*Article history:*
Received 29 June 2021
Received in revised form
27 August 2021
Accepted 05 September 2021

*Keywords:*
Coupled hygrothermal
Transient response
Functionally graded material
Hollow cylinder
Differential quadrature method

**Abstract**

The Distribution of displacements and stresses in a finite length hollow cylinder made of functionally graded material (FGM) subjected to coupled hygrothermal loading was investigated. The simply supported cylinder was under a transient coupled hygrothermal loading. Furthermore, the internal pressure and viscoelastic foundation can be considered for the cylinder. The coupled equations of heat and moisture transfer and motion equations of the cylinder were solved employing the Fourier series expansion method, the differential quadrature method (DQM), and the Newmark method along the longitudinal direction, the radial direction, and the time domain, respectively. Finally, the distribution of temperature, humidity, deformations, and stresses was obtained. The effects of coupled and uncoupled hygrothermal loading, grading index, hygrothermal boundary condition, and viscoelastic foundation are illustrated in the numerical examples. The results show that the FGM cylinder touches the temperature balance before using the uncoupled model rather than the coupled model. Moreover, by serving the time, the radial displacement, and maximum hoop stress increase, and longitudinal displacement decreases to reach steady-state condition.

**Nomenclature**

| | | | |
|---|---|---|---|
| $c_{ij}$ | Component of the stiffness matrix | $h_{LV}$ | Heat of phase change [kJ/kg] |
| E | Elastic moduli | L | Length of cylinder |
| T | Temperature distribution [K] | $\varepsilon$ | Hygrothermal index |
| M | Moisture concentration [°M] | $c_p$ | Heat capacity [J/kgK] |
| $\sigma_i$ | Normal stress component [N/m$^2$] | $c_m$ | Moisture capacity [J/kg°M] |
| $\tau_{ij}$ | Shear stress component [N/m$^2$] | a | Inner radius [m] |
| $\rho$ | Mass density [kg/m$^3$] | $b$ | Outer radius [m] |
| $\zeta$ | Conduction coefficient of moisture [kg/ms°M] | k | Thermal conductivity coefficients [W/mK] |
| $\alpha$ | Thermal expansion coefficients [1/K] | $u_i$ | Displacements [m] |
| $\xi_i$ | Moisture expansion coefficients [m$^3$/kg] | $\varepsilon_i$ | Components of strain |
| $\beta$ | Grading index | $C_d$ | Viscoelastic coefficient |
| $\xi_d$ | Ratio of vapor diffusion coefficient to coefficient of total moisture diffusion | $A_{ij}^{(n)}$ | Weighting coefficients for the $n_{th}$-order derivatives |

*Corresponding author: M. Saadatfar (Assistant Professor)
E-mail address: m.saadatfar@gmail.com
http://dx.doi.org/10.22084/jrstan.2021.24755.1189
ISSN: 2588-2597

| | | | |
|---|---|---|---|
| $\nu$ | Poison ratio | $k_L$ | Winkler's modulus |
| $\gamma$ | Heat of absorption or desorption [kJ/kg] | N | Number of grid points along the $x$-direction |

## 1. Introduction

FGMs have been employed in industrial structures owing to their excellent thermomechanical properties. The idea of FGM is proper to various engineering areas such as nuclear energy, aerospace vehicle, chemical plant, and electronics [1-3]. In the last decade, many researchers tried to study the behavior of FGMs in various environmental conditions [4, 5]. Due to usages of industrial structures subjected to various environmental conditions and loads, disclosing the influence of humidity, thermal environment, and mechanical loads on their behavior is a new topic in the literature.

Stress analysis of FGM cylinders and cylindrical shells is the topic of many research works in the literature. Jabbari et al. [6] analyzed thermo-mechanical stresses in FGM thick-walled cylinders under non-axisymmetric steady-state loads. Jabbari et al. [7] studied the three-dimensional thermo-mechanical stresses in FGM short hollow cylinders. Ootao and Tanigawa [8] presented the transient thermoelastic analysis of FGM thick-walled cylinders subjected to asymmetrical thermal boundary conditions. Transient heat conduction in two-dimensional FGM short hollow cylinders was analyzed by Asghari and Akhlaghi [9]. Loghman et al. [10] analyzed the time-dependent creep behavior of FGM hollow cylinders subjected to a magnetic field and thermo-mechanical loads. Dai and Rao [11] presented an investigation for the transient behavior of thick-walled FGM cylinders under radially symmetric loads. Zamani Nejad and Davoudi Kashkoli [12] presented time-dependent thermo-mechanical creep analysis for a rotating hollow cylinder made of FGM. Using a semi-analytical solution, Jabbari et al. [13] analyzed rotating variable thickness of FGM cylindrical shells subjected to thermal loads and internal non-uniform pressure. Davoudi Kashkoli et al. [14] analyzed time-dependent creep stresses and deformation of FGM cylinders subjected to thermal loading. The transient thermo-mechanical behavior of a short hollow cylinder made of two-dimensional FGM was investigated by Najibi and Talebitooti [15]. A new 2D-FGM material model based on the Mori-Tanaka scheme and third-order transition function was expressed for a short hollow cylinder by Najibi [16]. Hajisadeghian et al. [17] used an analytical solution to analyze stresses in an axisymmetric double-layered cylinder made of FGM and homogeneous layers under magneto-thermo-mechanical loads. The problem of time-dependent responses of a rotating thick-walled cylinder made of Functionally Graded Magneto-Electro-Elastic (FGMEE) was analyzed by Saadatfar [18]. Yarimpabuc obtained a closed-form solution for transient thermal stress response of FGM hollow cylinders subjected to temperature gradient under a periodic rotation [19]. A thermo-elastic analysis for rotating variable thickness FGM cylindrical shells subjected to thermal and mechanical loads was presented by Jabbari and Zamani Nejad [20].

Analysis of multilayered composites, FGMs, and smart materials in the hygrothermal environmental condition is of interest for many researchers. Using an analytical method, Akbarzadeh and Chen [21] investigated the hygro-thermo-elastic stresses in FGPM cylinders. Allam et al. [22] analyzed the hygro-thermo-electro-elastic stresses in thick-walled piezoelectric cylinders. Saadatfar and Aghaie-Khafri [23] evaluated hygrothermal stresses and displacements in FGMEE thick-walled spheres using an analytical method. Saadatfar and Aghaie Khafri [24] analyzed a hybrid cylindrical shell with FGM core and FGPM layers under hygro-thermo-mechanical loadings. They explained that the inhomogeneity index has a significant effect on the authority of the FGPM actuator and sensor under multifield loading. Saadatfar and Aghaie-Khafri [25] analyzed the hygrothermal response of FGM cylindrical shells with FGPM facesheets. Later, hygro-thermo-magneto-electro-elastic analysis of this problem was presented by saadatfar [26, 27]. Saadatfar [28] investigated the history of electric and magnetic potentials, radial and hoop stresses, and radial deformation of thick-walled FGMEE cylinders subjected to an axisymmetric hygro-thermo-magneto-electro-mechanical loading. Saadatfar [29] analytically solved the problem of the time-dependent behavior of a piezomagnetic rotating thick-walled cylinder subjected to axisymmetric multi-physical loads. Later, Saadatfar [30] investigated the temperature distribution obtained from coupled and uncoupled hygrothermal models in FGM cylinders. Using DQM, Saadatfar [31] analyzed the transient hygrothermal stress of a simply-supported short-length FGPM cylinder.

Due to the complexity of coupled hygrothermal equations, the uncoupled hygrothermal equations have been supposed in most of the published articles. Using the finite difference method, Yang et al. [32] solved the transient coupled hygrothermal problem of a long cylinder. An investigation on the hygrothermal stresses and deformation of a rotating FGPM disc under coupled hygrothermal loading was presented by Dai et al. [33]. Dai et al. [34] studied the coupled hygrothermal stress and displacement of a rotating porous disk made of functionally graded carbon nanotube-reinforced composites. The transient coupled hygrothermal and mechanical behavior of a long cylinder under sudden hygrothermal loadings was studied Peng et al. [35]. Peng et al. [36] analyzed the transient response of a long porous cylinder subjected to coupled hygrothermal conditions.

Literature review reveals that there is not any reported work on transient responses of a finite length FGM cylinder subjected to coupled hygrothermal conditions. Thus, for the first time, the coupled equations of heat conduction and moisture diffusion together with motion equations were considered for finite length FGM cylinder. Therefore, the novelty of this work is to consider the transient coupled hygrothermal loading in FGM cylinders. All of the reported articles in the literature worked on transient thermal and transient uncoupled hygrothermal loading. No published article is there to investigate the coupled hygrothermal stress and compare it with uncoupled hygrothermal stress in FGM cylinders.

## 2. Coupled Hygrothermal Field

Consider a hollow cylinder with interior and exterior radius $a$ and $b$, respectively. Since the finite or long length assumption for the cylinder depends on the ratio of radius to length [37], the finite length was assumed for the cylinder to have more general analysis. The FGM cylinder is located in a hygrothermal field. For the sake of simplifying, the material properties of the FGM are supposed to be a power-law function of radius as:

$$Y = Y'\left(\frac{r}{a}\right)^{\beta}, \qquad Y = E, k, \rho, \zeta, \alpha, \xi \tag{1}$$

where $\beta$ is the grading index and $Y$ and $Y'$ are material constants and corresponding values at the inside radius, respectively. Furthermore, $E, \rho, k$, $\zeta, \alpha$, and $\xi$ are the elastic moduli, mass density, coefficients of thermal conductivity, moisture diffusivity, thermal expansion, and moisture expansion, respectively.

### *2.1. Basic Equations*

The coupled hygrothermal equations are expressed as [38]:

$$\begin{aligned}
&\nabla\cdot(k\nabla T) + \rho c_m(\xi_D h_{LV}+\gamma)\frac{\partial M}{\partial t} = \rho c_P\frac{\partial T}{\partial t}\\
&\rho c_m\frac{\partial M}{\partial t} = \nabla\cdot(\zeta\nabla M) + \nabla\cdot(\varepsilon\zeta\nabla T)
\end{aligned} \tag{2}$$

where, $M$, $T$, $c_m$, $c_p$, $\varepsilon$, $\gamma$, $h_{LV}$ and $\xi_d$ are the temperature, moisture, moisture capacity, heat capacity, hygrothermal index, the heat of absorption, the heat of phase change, and the ratio of vapor diffusion coefficient to coefficient of total moisture diffusion, respectively. It should be mentioned that the uncoupled hygrothermal is reached if the term $\rho c_m(\xi_D h_{LV}+\gamma)\dot{M}$ in the first equation and the term $\nabla\cdot(\varepsilon\xi\nabla T)$ in the second equation are omitted. Considering these terms is the difference between the present investigation with the reported investigations in the literature. Considering the cylindrical coordinate system, Eq. (2) can be rewritten as:

$$\begin{aligned}
&\frac{1}{r}\frac{\partial}{\partial r}\left(rk_r\frac{\partial T}{\partial r}\right) + \frac{1}{r^2}\frac{\partial}{\partial\theta}\left(k_\theta\frac{\partial T}{\partial\theta}\right) + \frac{\partial}{\partial z}\left(k_z\frac{\partial T}{\partial z}\right) =\\
&\qquad \rho c_P\frac{\partial T}{\partial t} - [\rho c_m(\xi_D h_{LV}+\gamma)]\frac{\partial M}{\partial t}\\
&\frac{1}{r}\frac{\partial}{\partial r}\left(r\zeta_r\frac{\partial M}{\partial r}\right) + \frac{1}{r^2}\frac{\partial}{\partial\theta}\left(\zeta_\theta\frac{\partial M}{\partial\theta}\right) + \frac{\partial}{\partial z}\left(\zeta_z\frac{\partial M}{\partial z}\right)\\
&+\frac{1}{r}\frac{\partial}{\partial r}\left(r\varepsilon\zeta_r\frac{\partial T}{\partial r}\right) + \frac{1}{r^2}\frac{\partial}{\partial\theta}\left(\varepsilon\zeta_\theta\frac{\partial T}{\partial\theta}\right)\\
&+\frac{\partial}{\partial z}\left(\varepsilon\zeta_z\frac{\partial T}{\partial z}\right) = \rho c_m\frac{\partial M}{\partial t}
\end{aligned} \tag{3}$$

Due to the axisymmetric condition, the terms include derivative respect to $\theta$ are vanished. By using Eq. (1), one has:

$$\begin{aligned}
&\left(k'_r\left(\frac{\partial^2}{\partial r^2} + \frac{\beta+1}{r}\frac{\partial}{\partial r}\right) + k'_z\frac{\partial^2}{\partial z^2}\right)T\\
&= \left(\frac{r}{a}\right)^{\beta}\rho' c'_p\frac{\partial T}{\partial t} - \left(\frac{r}{a}\right)^{\beta}\rho' c'_m(\xi_D h_{LV}+\gamma)\frac{\partial M}{\partial t}\\
&\left(\zeta'_r\left(\frac{\partial^2}{\partial r^2} + \frac{\beta+1}{r}\frac{\partial}{\partial r}\right) + \zeta'_z\frac{\partial^2}{\partial z^2}\right)M + \left(\varepsilon\zeta'_r\left(\frac{\partial^2}{\partial r^2}\right.\right.\\
&\left.\left.+\frac{\beta+1}{r}\frac{\partial}{\partial r}\right) + \varepsilon\zeta'_z\frac{\partial^2}{\partial z^2}\right)T = \left(\frac{r}{a}\right)^{\beta}\rho' c'_m\frac{\partial M}{\partial t}
\end{aligned} \tag{4}$$

The initial conditions of the hygrothermal field are considered as:

$$T(r,z,0) = 0, M(r,z,0) = 0 \tag{5}$$

The boundary conditions of hygrothermal field can be considered as:

$$\begin{aligned}
&T(a,z,t) = T_a, && T(b,z,t) = T_b\\
&M(a,z,t) = M_a, && M(b,z,t) = M_b\\
&T(r,0,t) = 0, && T(r,L,t) = 0\\
&M(r,0,t) = 0, && M(r,L,t) = 0
\end{aligned} \tag{6}$$

### *2.2. Solution Method*

The solutions of the coupled hygrothermal problem satisfying the hygrothermal boundary conditions at the end faces of the cylinder can be taken as:

$$T(r,z,t)=\sum_{n=1}^{\infty}\bar{T}_n(r,t)\sin(p_n z)$$
$$M(r,z,t)=\sum_{n=1}^{\infty}\bar{M}_n(r,t)\sin(p_n z) \tag{7}$$

where, $p_n = n\pi/L$. Using Eq. (7), Eq. (4) can be rewritten as:

$$\left(k'_r\left(\frac{\partial^2}{\partial r^2}+\frac{\beta+1}{r}\frac{\partial}{\partial r}\right)-k'_z p_n^2\right)\bar{T} = \left(\frac{r}{a}\right)^{\beta}\rho' c'_p\frac{\partial T}{\partial t}-\left(\frac{r}{a}\right)^{\beta}\rho c'_m(\xi_D h_{LV}+\gamma)\frac{\partial \bar{M}}{\partial t}$$
$$\left(\zeta'_r\left(\frac{\partial^2}{\partial r^2}+\frac{\beta+1}{r}\frac{\partial}{\partial r}\right)-\zeta'_z p_n^2\right)\bar{M}+\left(\varepsilon\zeta'_r\left(\frac{\partial^2}{\partial r^2}+\frac{\beta+1}{r}\frac{\partial}{\partial r}\right)-\varepsilon\zeta'_z p_n^2\right)\bar{T}=\left(\frac{r}{a}\right)^{\beta}\rho' c'_m\frac{\partial \bar{M}}{\partial t} \tag{8}$$

According to DQM, the nth-order derivative of the function $f(x)$ can be estimated as [26]:

$$\frac{d^n f(x_i)}{dx^n}=\sum_{j=1}^{N}A_{ij}^{(n)}f(x_j)$$
$$i=1,\cdots,N,\quad n=1,\cdots,N-1 \tag{9}$$

where, the first and the second-order weighting coefficients can be expressed as [26]:

$$A_{ij}^{(1)}=\frac{\Pi(x_i)}{(x_i-x_j)\cdot\Pi(x_j)}\quad i,j=1,\cdots,N \text{ and } j\neq i$$
$$A_{ij}^{(2)}=2\left[A_{ii}^{(1)}\cdot A_{ij}^{(1)}-\frac{A_{ij}^{(1)}}{x_i-x_j}\right]\quad 2\le n\le N-1$$
$$A_{ii}^{(1)}=-\sum_{\substack{j=1\\ j\neq i}}^{N}A_{ij}^{(1)}\quad k=1,\cdots,N-1$$
$$\Pi(x_i)=\prod_{\substack{j=1\\ j\neq i}}^{N}(x_i-x_j) \tag{10}$$

Moreover, the Chebyshev–Gauss–Lobatto points can be used as [24]:

$$x_i=\frac{L}{2}\left(1-\cos\left[\frac{(i-1)\pi}{(N-1)}\right]\right)\quad i=1,2,\cdots,N \tag{11}$$

Using DQM, the equations of coupled hygrothermal can be expressed as:

$$k'_r\left(\sum_{j=1}^{N}A_{ij}^{(2)}+\frac{\beta+1}{r_i}\sum_{j=1}^{N}A_{ij}^{(1)}\right)\bar{T}_j-k'_z p_n^2\bar{T}_i = \left(\frac{r_i}{a}\right)^{\beta}\rho' c'_p\frac{\partial \bar{T}_i}{\partial t}-\left(\frac{r_i}{a}\right)^{\beta}\rho' c'_m(\xi_D h_{LV}+\gamma)\frac{\partial \bar{M}_i}{\partial t} \tag{12}$$

$$\zeta'_r\left(\sum_{j=1}^{N}A_{ij}^{(2)}+\frac{\beta+1}{r_i}\sum_{j=1}^{N}A_{ij}^{(1)}\right)\bar{M}_j-\zeta'_z p_n^2\bar{M}_i +\varepsilon\zeta'_r\left(\sum_{j=1}^{N}A_{ij}^{(2)}+\frac{\beta+1}{r_i}\sum_{j=1}^{N}A_{ij}^{(1)}\right)\bar{T}_j-\varepsilon\zeta'_z p_n^2\bar{T}_i = \left(\frac{r_i}{a}\right)^{\beta}\rho' c'_m\frac{\partial \bar{M}_i}{\partial t}$$

Now the Newmark method is selected for discretizing the time domain. The time domain is discretized by time step $\Delta t$. According to the Newmark method, the function $U(r,t)$ and its derivatives with respect to time can be approximated by [33]:

$$\ddot{U}(r_i,t_{i+1})=a_0(U(r_i,t_{i+1})-U(r_i,t_i))-a_1\dot{U}(r_i,t_i) - a_2\ddot{U}(r_i,t_i)-a_2\ddot{U}(r_i,t_i)$$
$$\dot{U}(r_i,t_{i+1})=\dot{U}(r_i,t_i)+a_3\ddot{U}(r_i,t_i)+a_4\ddot{U}(r_i,t_{i+1})$$
$$a_0=\frac{1}{\alpha_0\Delta t^2},\quad a_1=\frac{1}{\alpha_0\Delta t},\quad a_2=\frac{1}{2\alpha_0}-1,$$
$$a_3=\Delta t(1-\delta_0),\quad a_4=\delta_0\Delta t \tag{13}$$

where $\alpha_0=\dfrac{1}{4}$ and $\delta_0=\dfrac{1}{2}$ are used. Now, Eq. (12) can be rewritten in the form as:

$$k'_r\left(\sum_{j=1}^{N}A_{ij}^{(2)}+\frac{\beta+1}{r_i}\sum_{j=1}^{N}A_{ij}^{(1)}\right)\bar{T}_j(t_{k+1}) -\left(k'_z p_n^2+a_4a_0\left(\frac{r_i}{a}\right)^{\beta}\rho' c'_p\right)\bar{T}_i(t_{k+1}) +a_4a_0\left(\frac{r_i}{a}\right)^{\beta}\rho' c'_m(\xi_D h_{LV}+\gamma)\bar{M}_i(t_{k+1})$$
$$=\left(\frac{r_i}{a}\right)^{\beta}\rho' c'_p\big(\dot{\bar{T}}_i(t_k)+a_3\ddot{\bar{T}}_i(t_k) - a_4a_0\bar{T}(t_k)-a_4a_1\dot{\bar{T}}_i(t_k)-a_4a_2\ddot{\bar{T}}_i(t_k)\big) -\left(\frac{r_i}{a}\right)^{\beta}\rho' c'_m(\xi_D h_{LV}+\gamma)(\dot{\bar{M}}_i(t_k)+a_3\ddot{\bar{M}}_i(t_k) - a_4a_0\bar{M}_i(t_k)-a_4a_1\dot{\bar{M}}_i(t_k)-a_4a_2\bar{M}_i(t_k)\big) \tag{14}$$

$$\zeta_r'\left(\sum_{j=1}^{N}A_{ij}^{(2)}+\frac{\beta+1}{r_i}\sum_{j=1}^{N}A_{ij}^{(1)}\right)\bar{M}_j(t_{k+1})$$
$$-\left(\zeta_z' p_n^2+a_4a_0\left(\frac{r_i}{a}\right)^{\beta}\rho' c_m'\right)\bar{M}_i(t_{k+1})$$
$$+\varepsilon\zeta_r'\left(\sum_{j=1}^{N}A_{ij}^{(2)}+\frac{\beta+1}{r_i}\sum_{j=1}^{N}A_{ij}^{(1)}\right)\bar{T}_j(t_{k+1})$$
$$-\varepsilon\zeta_z' p_n^2\bar{T}_i(t_{k+1})=\left(\frac{r_i}{a}\right)^{\beta}\rho' c_m'\big(\,\dot{\bar{M}}_i(t_k)+a_3\ddot{\bar{M}}_i(t_k)$$
$$-a_4a_0\bar{M}_i(t_k)-a_4a_1\dot{\bar{M}}_i(t_k)-a_4a_2\ddot{\bar{M}}_i(t_k)-\big) \quad (15)$$

Now, employing an iterative method, the resultant system of algebraic equations can be solved in each time step.

## 3. Basic Formulation of Stress Problem

### *3.1. Basic Equations*

Stresses in the FGM cylinder in terms of strains can be written as [25]:

$$\begin{aligned}
&\sigma_r=c_{11}\varepsilon_r+c_{12}\varepsilon_\theta+c_{13}\varepsilon_z-\lambda_rT-\bar{w}_rM\\
&\sigma_\theta=c_{21}\varepsilon_r+c_{22}\varepsilon_\theta+c_{23}\varepsilon_z-\lambda_\theta T-\bar{w}_\theta M\\
&\sigma_z=c_{31}\varepsilon_r+c_{32}\varepsilon_\theta+c_{33}\varepsilon_z-\lambda_zT-\bar{w}_zM\\
&\tau_{rz}=c_{55}\gamma_{zr}\\
&\lambda_r=c_{11}\alpha_r+c_{12}\alpha_\theta+c_{13}\alpha_z\\
&\lambda_\theta=c_{12}\alpha_r+c_{22}\alpha_\theta+c_{23}\alpha_z\\
&\lambda_z=c_{13}\alpha_r+c_{23}\alpha_\theta+c_{33}\alpha_z\\
&\bar{w}_r=c_{11}\xi_r+c_{12}\xi_\theta+c_{13}\xi_z\\
&\bar{w}_\theta=c_{12}\xi_r+c_{22}\xi_\theta+c_{23}\xi_z\\
&\bar{w}_z=c_{13}\xi_r+c_{23}\xi_\theta+c_{33}\xi_z
\end{aligned} \quad (16)$$

where, $c_{ij}$, $\sigma_i$, $\tau_i$, $\varepsilon_i$, $\lambda_i$, and $\bar{w}_i$ are components of the stiffness matrix, normal stress, shear stress, normal strain, thermal modulus, and moisture modulus, respectively. The strain-displacement relations are taken as [20]:

$$\varepsilon_r=\frac{\partial u_r}{\partial r},\quad \varepsilon_\theta=\frac{u}{r}\quad \varepsilon_z=\frac{\partial u_z}{\partial z},$$
$$\gamma_{zr}=\left(\frac{\partial u_r}{\partial z}+\frac{\partial u_z}{\partial r}\right) \quad (17)$$

Employing Eq.(1) and Eq.(17) in Eq.(16) yields:

$$\begin{aligned}
&\sigma_r=\left(\frac{r}{a}\right)^{\beta}\left[c_{11}'\frac{\partial u_r}{\partial r}+c_{12}'\left(\frac{u_r}{r}\right)+c_{13}'\frac{\partial u_z}{\partial z}\right]\\
&\quad-\lambda_r'\left(\frac{r}{a}\right)^{2\beta}T-\bar{w}_r'\left(\frac{r}{a}\right)^{2\beta}M\\
&\sigma_\theta=\left(\frac{r}{a}\right)^{\beta}\left[c_{12}'\frac{\partial u_r}{\partial r}+c_{22}'\left(\frac{u_r}{r}\right)+c_{23}'\frac{\partial u_z}{\partial z}\right]\\
&\quad-\lambda_\theta'\left(\frac{r}{a}\right)^{2\beta}T-\bar{w}_\theta'\left(\frac{r}{a}\right)^{2\beta}M\\
&\sigma_z=\left(\frac{r}{a}\right)^{\beta}\left[c_{13}'\frac{\partial u_r}{\partial r}+c_{23}'\left(\frac{u_r}{r}\right)+c_{33}'\frac{\partial u_z}{\partial z}\right]\\
&\quad-\lambda_z'\left(\frac{r}{a}\right)^{2\beta}T-\bar{w}_z'\left(\frac{r}{a}\right)^{2\beta}M\\
&\tau_{rz}=\left(\frac{r}{a}\right)^{\beta}\left[c_{55}'\left(\frac{\partial u_r}{\partial z}+\frac{\partial u_z}{\partial r}\right)\right]
\end{aligned} \quad (18)$$

Equations of motion for axisymmetric deformations of the cylinder are expressed as [27]:

$$\begin{aligned}
&\frac{\partial\sigma_r}{\partial r}+\frac{\partial\tau_{rz}}{\partial z}+\frac{\sigma_r-\sigma_\theta}{r}=\rho\frac{\partial^2u_r}{\partial t^2}\\
&\frac{\partial\tau_{rz}}{\partial r}+\frac{\partial\sigma_z}{\partial z}+\frac{\tau_{rz}}{r}=\rho\frac{\partial^2u_z}{\partial t^2}
\end{aligned} \quad (19)$$

Substituting E. (18) in Eq. (19) yields:

$$\left(c_{11}'\frac{\partial^2}{\partial r^2}+\frac{(\beta+1)c_{11}'}{r}\frac{\partial}{\partial r}+\frac{\beta c_{12}'-c_{22}'}{r^2}+c_{55}'\frac{\partial^2}{\partial z^2}\right)u_r$$
$$+\left(\frac{1}{r}((\beta+1)c_{13}'-c_{23}')\frac{\partial}{\partial z}+(c_{13}'+c_{55}')\frac{\partial}{\partial r\partial z}\right)u_z$$
$$+\left(\frac{r}{a}\right)^{\beta}\left(\frac{1}{r}(\lambda_\theta'-(2\beta+1)\lambda_r')-\lambda_r'\frac{\partial}{\partial r}\right)T$$
$$+\left(\frac{r}{a}\right)^{\beta}\left(\frac{1}{r}(\bar{w}_\beta'-(2\beta+1)\bar{w}_r')-\bar{w}_r'\frac{\partial}{\partial r}\right)M=\rho'\frac{\partial^2u_r}{\partial t^2} \quad (20)$$

$$\left(\frac{1}{r}((\beta+1)c_{55}'+c_{23}')\frac{\partial}{\partial z}+(c_{55}'+c_{13}')\frac{\partial}{\partial r\partial z}\right)u_r$$
$$+\left(\frac{\beta+1}{r}c_{55}'\frac{\partial}{\partial r}+c_{55}'\frac{\partial^2}{\partial r^2}+c_{33}'\frac{\partial^2}{\partial z^2}\right)u_z$$
$$-\lambda_z'\left(\frac{r}{a}\right)^{\beta}\frac{\partial}{\partial z}T-\bar{w}_z'\left(\frac{r}{a}\right)^{\beta}\frac{\partial}{\partial z}M=\rho'\frac{\partial^2u_z}{\partial t^2} \quad (21)$$

The simply supported boundary conditions were considered for the cylinder. Additionally, the internal pressure and viscoelastic foundation can be taken for the cylinder. Therefore, the boundary conditions can be expressed as:

$$\begin{aligned} &u_r = \sigma_z = 0 \quad \text{at} \quad z = 0, L \\ &\sigma_r = -P_a, \quad \tau_{zr} = 0, \quad \text{at} \quad r = a \\ &\sigma_r = -k_L u_r - C_d \frac{\partial u_r}{\partial t}, \quad \tau_{zr} = 0, \quad \text{at} \quad r = d \end{aligned} \tag{22}$$

where $k_L$ and $C_d$ are Winkler modulus and viscoelastic coefficient, respectively.

### *3.2. Solution Method*

The solution satisfying the boundary conditions can be taken as:

$$\begin{aligned} u_r(r,z,t) &= \sum_{n=1}^{\infty} U_r(r,t)\sin(b_n z) \\ u_z(r,z,t) &= \sum_{n=1}^{\infty} U_z(r,t)\cos(b_n z) \end{aligned} \tag{23}$$

Substituting Eq. (23) into Eqs. (20) and (21) yields:

$$\begin{aligned} &\left(c'_{11}\frac{\partial^2}{\partial r^2} + \frac{(\beta+1)c'_{11}}{r}\frac{\partial}{\partial r} + \frac{\beta c'_{12} - c'_{22}}{r^2} - c'_{55}b^2 n\right)U_r \\ &- \left(\frac{b_n}{r}\left((\beta+1)c'_{13} - c'_{23}\right) + b_n(c'_{13} + c'_{55})\frac{\partial}{\partial r}\right)U_z \\ &+ \left(\frac{r}{a}\right)^{\beta}\left(\frac{1}{r}(\lambda'_\theta - (2\beta+1)\lambda'_r) - \lambda'_r\frac{\partial}{\partial r}\right)\bar{T} \\ &+ \left(\frac{r}{a}\right)^{\beta}\left(\frac{1}{r}(\bar{w}'_\beta - (2\beta+1)\bar{w}'_r) - \bar{w}'_r\frac{\partial}{\partial r}\right)\bar{M} \\ &= \rho'\frac{\partial^2 U_r}{\partial t^2} \end{aligned} \tag{24}$$

$$\begin{aligned} &\left(\frac{b_n}{r}\left((\beta+1)c'_{55} + c'_{23}\right) + b_n(c'_{55} + c'_{13})\frac{\partial}{\partial r}\right)U_r \\ &+ \left(\frac{\beta+1}{r}c'_{55}\frac{\partial}{\partial r} + c'_{55}\frac{\partial^2}{\partial r^2} + c'_{33}b_n^2\right)U_z \\ &- \lambda'_z b_n\left(\frac{r}{a}\right)^{\beta}\bar{T} - \bar{w}'_z b_n\left(\frac{r}{a}\right)^{\beta}\bar{M} = \rho'\frac{\partial^2 u_z}{\partial t^2} \end{aligned} \tag{25}$$

Using the DQM, Eqs. (24) and (25) can be written as:

$$\begin{aligned} &\left(c'_{11}\sum_{j=1}^{N}A_{ij}^{(2)} + \frac{(\beta+1)c'_{11}}{r_i}\sum_{j=1}^{N}A_{ij}^{(1)} + \frac{\beta c'_{12} - c'_{22}}{r_i^2} - c'_{55}b^2 n\right)U_{rj} \\ &- \left(\frac{b_n}{r_i}\left((\beta+1)c'_{13} - c'_{23}\right) + b_n^2(c'_{13} + c'_{55})\sum_{j=1}^{N}A_{ij}^{(1)}\right)U_{zj} \\ &+ \left(\frac{r_i}{a}\right)^{\beta}\left(\frac{1}{r}(\lambda'_\theta - (2\beta+1)\lambda'_r) - \lambda'_r\sum_{j=1}^{N}A_{ij}^{(2)}\right)\bar{T}_j \\ &+ \left(\frac{r_i}{a}\right)^{\beta}\left(\frac{1}{r}(\bar{w}'_\theta - (2\beta+1)\bar{w}'_r) - \bar{w}'_r\sum_{j=1}^{N}A_{ij}^{(1)}\right)\bar{M}_j \\ &= \rho'\frac{\partial^2 U_r}{\partial t^2} \end{aligned} \tag{26}$$

$$\begin{aligned} &\left(\frac{b_n}{r_i}\left((\beta+1)c'_{55} + c'_{23}\right) + b_n(c'_{55} + c'_{13})\sum_{j=1}^{N}A_{ij}^{(1)}\right)U_{rj} \\ &+ \left(\frac{\beta+1}{r_i}c'_{55}\sum_{j=1}^{N}A_{ij}^{(1)} + c'_{55}\sum_{j=1}^{N}A_{ij}^{(2)} - c'_{33}b_n^2\right)U_{zj} \\ &- \lambda'_z b_n\left(\frac{r_i}{a}\right)^{\beta}\bar{T}_j - \bar{w}'_z b_n\left(\frac{r_i}{a}\right)^{\beta}\bar{M}_j = \rho'\frac{\partial^2 U_z}{\partial t^2} \end{aligned} \tag{27}$$

Employing the Newmark method, Eqs. (26) and (27) can be written as:

$$\begin{aligned} &\left(c'_{11}\sum_{j=1}^{N}A_{ij}^{(2)} + \frac{(\beta+1)c'_{11}}{r_i}\sum_{j=1}^{N}A_{ij}^{(1)} + \frac{\beta c'_{12} - c'_{22}}{r_i^2} - c'_{55}b^2 n - \rho' a_0\right)U_{rj}(t_{k+1}) \\ &- \left(\frac{b_n}{r_i}\left((\beta+1)c'_{13} - c'_{23}\right) + b_n^2(c'_{13} + c'_{55})\sum_{j=1}^{N}A_{ij}^{(1)}\right)U_{zj}(t_{k+1}) \\ &+ \left(\frac{r_i}{a}\right)^{\beta}\left(\frac{1}{r}(\lambda'_\theta - (2\beta+1)\lambda'_r) - \lambda'_r\sum_{j=1}^{N}A_{ij}^{(1)}\right)\bar{T}_j(t_{k+1}) \\ &+ \left(\frac{r_i}{a}\right)^{\beta}\left(\frac{1}{r_i}(\bar{w}'_\theta - (2\beta+1)\bar{w}'_r) - \bar{w}'_r\sum_{i=1}^{N}A_{ij}^{(1)}\right)\bar{M}_j(t_{k+1}) \\ &= -\rho'(a_0 U_r(t_k) + a_1\dot{U}_r(t_k) + a_2\ddot{U}_r(t_k)) \end{aligned} \tag{28}$$

$$\begin{aligned} &\left(\frac{b_n}{r_i}\left((\beta+1)c'_{55} + c'_{23}\right) + b_n(c'_{55} + c'_{13})\sum_{j=1}^{N}A_{ij}^{(1)}\right)U_{rj}(t_{k+1}) \\ &+ \left(\frac{\beta+1}{r_i}c'_{55}\sum_{j=1}^{N}A_{ij}^{(1)} + c'_{55}\sum_{j=1}^{N}A_{ij}^{(2)} - c'_{33}b_n^2 - \rho' a_0\right)U_{zj}(t_{k+1}) \end{aligned}$$

$$- \lambda'_z b_n \left(\frac{r_i}{a}\right)^{\beta} \bar{T}_i(t_{k+1}) - \bar{w}'_z b_n \left(\frac{r_i}{a}\right)^{\beta} \bar{M}_i(t_{k+1})$$
$$= \rho'(a_0 U_z(t_k) + a_1 \dot{U}_z(t_k) + a_2 \ddot{U}_z(t_k)) \quad (29)$$

Similarly, the method can be employed for boundary conditions. Therefore, the inner and outer boundary conditions can be written as:

$$\left(c'_{11} \sum_{j=1}^{N} A_{1j}^{(1)} + \frac{c'_{12}}{a}\right) U_{rN} - c'_{13} b_n U_{z1} - \lambda'_r \bar{T}_1$$
$$- \bar{w}'_r \bar{M}_1 = -P_a, \quad (30)$$

$$c'_{55}\left(b_n U_{r1} + \sum_{j=1}^{N} A_{1j}^{(1)} U_{zj}\right) = 0 \quad (31)$$

$$\left(c'_{11} \sum_{j=1}^{N} A_{1j}^{(1)} + \frac{c'_{12}}{a}\right) U_{rj} - c'_{13} b_n U_{zN} - \lambda'_r \bar{T}_N$$
$$- \bar{w}'_r \bar{M}_N + k_L U_{rN} + C_d a_4 a_0 U_N(t_{k+1})$$
$$= -C_d(\dot{U}_N(t_k) + a_3 \ddot{U}_N(t_k) - a_4 a_0 U_N(t_k)$$
$$- a_4 a_1 \dot{U}_N(t_k) - a_4 a_2 \ddot{U}_N(t_k)) \quad (32)$$

$$c'_{55}\left(b_n U_{rN} + \sum_{j=1}^{N} A_{Nj}^{(1)} U_{zj}\right) = 0, \quad (33)$$

Domain ($d$) and boundary ($b$) degrees of freedom must be separated. Hence, equations together with boundary conditions can be considered in the matrix form as:

$$\begin{bmatrix} [Q_{bb}] & [Q_{bd}] \\ [Q_{db}] & [Q_{dd}] \end{bmatrix} \begin{Bmatrix} \{U_b\} \\ \{U_d\} \end{Bmatrix} = \begin{Bmatrix} \{F_b\} \\ \{F_d\} \end{Bmatrix} \quad (34)$$

where:

$$\{U_b\} = \{\{U_{rb}\}, \{U_{zb}\}\}^T$$
$$\{U_d\} = \{\{U_{rd}\}, \{U_{zd}\}\}^T \quad (35)$$

The matrix Eq. (34) can be reduced to the following system of algebraic equations by omitting the $U_b$:

$$[Q]\{U_d\} = \{F\}$$
$$[Q] = [Q_{dd}] - [Q_{db}][Q_{bb}]^{-1}[Q_{bd}] \quad (36)$$
$$\{F\} = \{F\}_d - [Q_{db}][Q_{bb}]^{-1}\{F_b\}$$

Employing direct or iterative methods, the solution of Eq. (36) can be found. In this problem, employing iterative methods such as the Gauss–Seidel method is recommended.

## 4. Numerical Results and Discussion

To disclose the effects of different parameters on the transient behavior of the FGM hollow cylinder, some numerical examples are presented in this section. Material constants to be used for the FGM cylinder are in Table 1 [6, 33, 35]. The length and inside and outside radius of the hollow cylinder were considered as $L = 1$m, $a = 0.2$m, and $b = 0.25$m. Some non-dimensional parameters are defined in the results as:

$$R = \frac{r-a}{b-a}, \quad u^* = \frac{u}{a}, \quad \sigma_i^* = \frac{\sigma_i}{P_a}, \ (i = r, \theta),$$
$$T^* = \frac{T}{T_a}, \quad M^* = \frac{M}{M_a} \quad (37)$$

The following relations were used for the FGM cylinder in the numerical examples:

$$c_{11} = c_{22} = c_{33} = \frac{E(1-\nu)}{(1+\nu)(1-2\nu)},$$
$$c_{12} = c_{13} = c_{23} = \frac{E}{(1+\nu)(1-2\nu)}, \quad (38)$$
$$c_{55} = \frac{E}{2(1+\nu)}$$

### 4.1. Validation of the Results

As mentioned in the literature review, there is no published research for transient coupled hygrothermal analysis of FGM cylinders. Therefore, the results were compared with the reported results for the FGM cylinder subjected to transient thermal loading. The temperature distribution through time was compared with Ref. [39]. Parameters are: $r_a = 0.5$m, $r_b = 1$m, $L = 1.5$m, $T_a = 100(1 - e^{-2t})$, $T_b = 0$. The material coefficients are in the cited reference. In another case, the shear stress distribution was compared with the reported one in Ref. [40]. In this case we have: $r_a = 1$m, $r_b = 1.5$m, $L = 1$m, $T_a = 100(1 - e^{-2t})$, $T_b = 0$. The used material constants can be found in the cited reference. The results are depicted in Fig. 1. As illustrated, the graphs show good agreement between the results.

**Table 1**
Material constants [6, 33, 35]

| | |
|---|---|
| E (GPa) | 66.2 |
| $\xi_d$ | 0.3 |
| $v$ | 0.3 |
| $\xi$ (m$^3$/kg) | $1.1 \times 10^{-4}$ |
| $\alpha$ (1/K) | $10.3 \times 10^{-6}$ |
| $\rho$(kg/m$^3$) | 5300 |
| $h_{LV}$ (kJ/kg) | 2500 |
| $\zeta_i$ (kg/ms°M) | $1.73 \times 10^{-8}$ |
| $\varepsilon$ (°M/K) | 2 |
| $c_m$(J/kg°M) | 0.01 |
| $\gamma$ | 0 |
| k(W/mk) | 18.1 |
| $c_p$(J/kgK) | 700 |

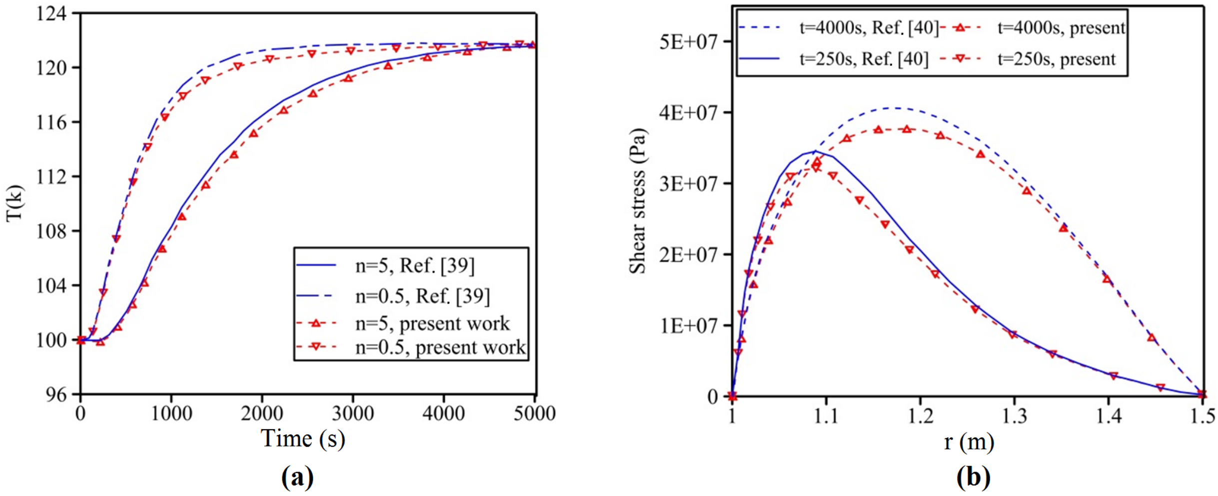


**Fig. 1.** Distribution of a) Temperature along time, and b) Shear stress along the radius.

### *4.2. Transient Coupled Hygrothermal Loading*

In this part, the distribution of temperature, moisture, displacements, and stresses under transient hygrothermal loading are studied. In this case there is: $T_a = 350$, $T_b = 0$, $M_a = 0.015$, $M_b = 0.01$. Fig. 2a depicts the temperature through the thickness. It shows that there is little difference between the coupled hygrothermal with the uncoupled model in temperature distribution. Fig. 2b shows the temperature distribution with time. Fig. 2b demonstrates that the FGM cylinder touches the temperature equilibrium former by employing the uncoupled model, and the temperature rises by serving the time before balance. Employing the coupled equations, the time to touch the balance is longer and the temperature first rises and then decreases before the balance. Before the balance state, the temperature with the coupled equations is higher than that by the uncoupled equations. Fig. 2c depicts the moisture distribution through the thickness. It is observed that the difference between the coupled and uncoupled models is more obvious in moisture rather than temperature. The above-mentioned behaviors have a good agreement with the reported behaviors in the rotating disc under coupled hygrothermal loading [34]. Dai et al. [34] reported that the FGPM disc touches the temperature equilibrium former by employing the uncoupled model, and the temperature rises by serving the time before balance.

Regarding the difference between the results under coupled and uncoupled model, for analyzing the dynamic conduction process it is vital to employ the coupled model. However, after the balance state, using the coupled model or uncoupled model has little effect. To have a better understanding of changes through time, Fig. 3 shows the distribution of temperature, radial displacement, hoop stress, and shear stress along the radius and time (coupled model).

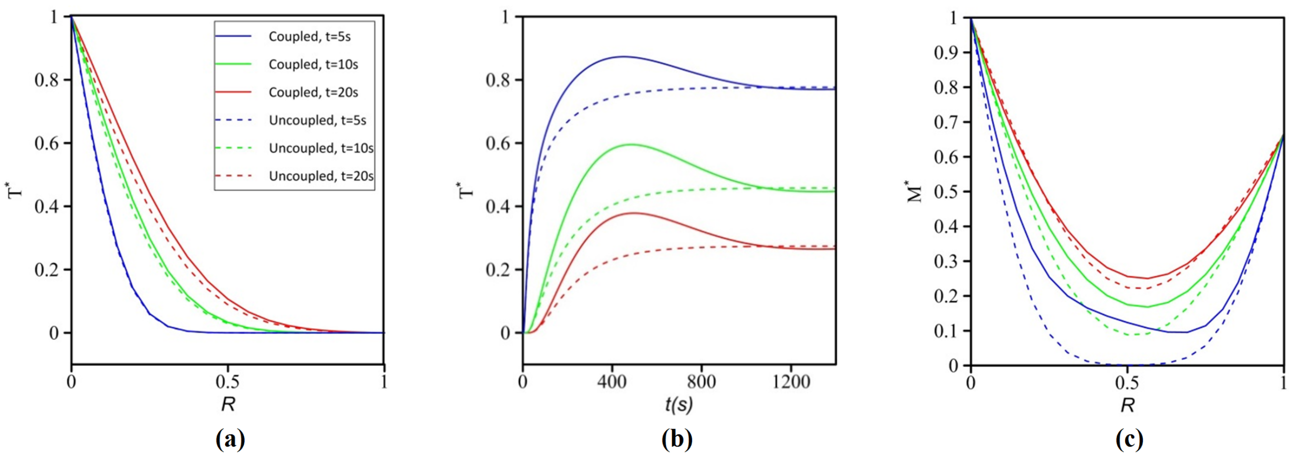


**Fig. 2.** Distribution of a) Temperature along the radius, b) Temperature along time, and c) Moisture along the radius, $\beta = 0.5$.

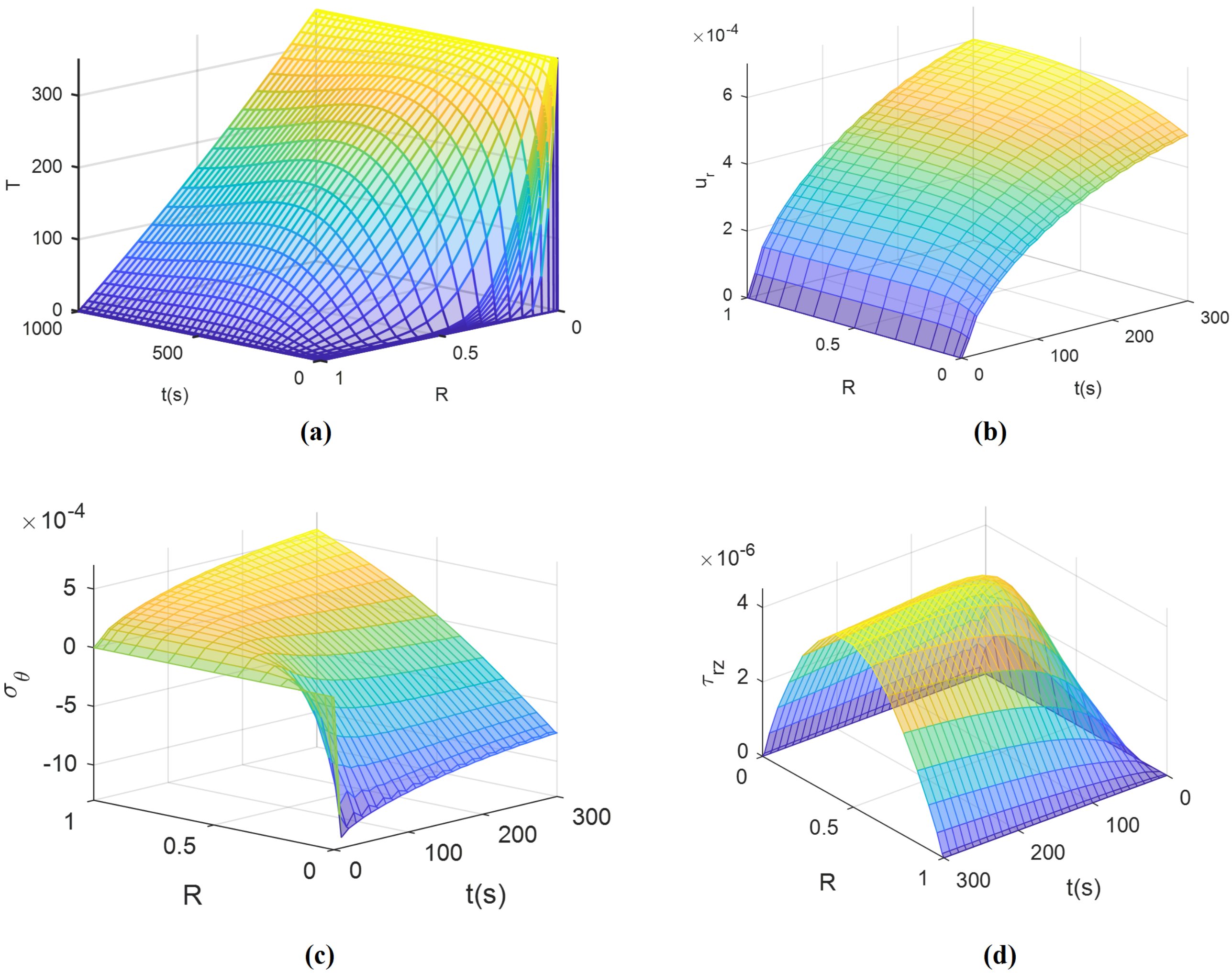


**Fig. 3.** Distribution of a) Temperature , b) Radial displacement, c) Hoop stress, and d) Shear stress for $\beta = 0.5$.

The distributions of stresses and displacements considering coupled and uncoupled models are depicted in Fig. 4. and Fig. 5. In this case there is: $w = 0$, $k_L = 0$, $C_d = 0$, $P_a = 0$, $T_a = 50$, $T_b = 0$, $M_a = 0.015$, $M_b = 0.01$. As shown in Fig. 4, the difference between the coupled and uncoupled models is not significant on the distribution of stresses and displacements. The maximum hoop stress increases by serving the time up to steady-state condition. By serving the time, radial displacement experiences an increase up to reaching steady-state conditions. Besides, the behavior of longitudinal displacement is the same. Fig. 5 demonstrates the distribution of stresses and displacement through the time for the point located at the middle of thickness. As shown, the shear stress, radial displacement, and absolute value of radial stress increase to reach steady-state condition. The hoop stress experiences an increase and then a decrease to reach the steady-state status. According to graphs, due to employing the boundary condition, the shear stress and radial stress reach balance condition earlier than hoop stress and radial displacement. The observed trend for the effect of steady-state hygrothermal loading was also reported in the literature for smart finite-length cylinders [26]. The grading index is the next parameter that its influence was investigated. The effect of the grading index is demonstrated in Figs. 6 and 7. The boundary conditions are as previous. According to Fig. 6, the negative grading index increases the temperature and moisture at the same point, while the effect of a positive grading index is vice versa. This trend is in agreement with the reported one by Bakhshizade et al. [41]. Furthermore, the negative grading index increases the balance temperature and the positive grading index reduces the balance temperature. Concerning Fig. 7, using a positive grading index increases the maximum of hoop stress; meanwhile, the effect of a negative grading index is converse. Moreover, using a positive grading index increases the shear stress. Reversely, a negative grading index causes a reduction in the shear stress. The effect of the grading index on the distribution of radial displacement is in contrast with its effect on the shear stress. This reduction of radial displacement by using a positive grading index rather than a negative grading index is in agreement with the reported trend for FGPM cylinders [42]. The graphs show that the difference between the coupled model and the uncoupled model is more considerable by using the negative grading index.

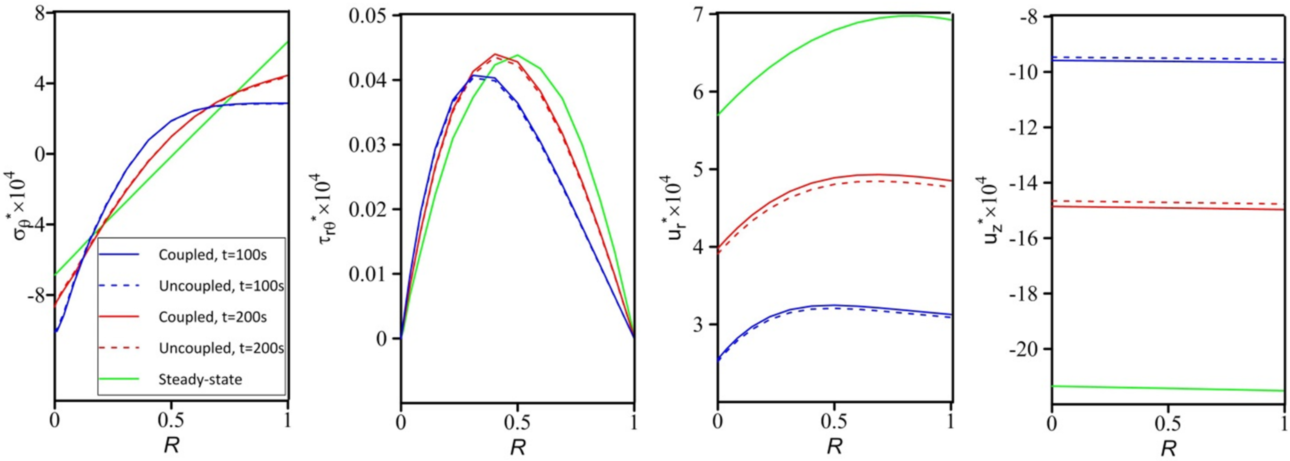


(a) (b) (c) (d)

**Fig. 4.** Distribution of a) Hoop, b) Shear stresses, c) Radial and d) Longitudinal displacements, $\beta = 0.5$.

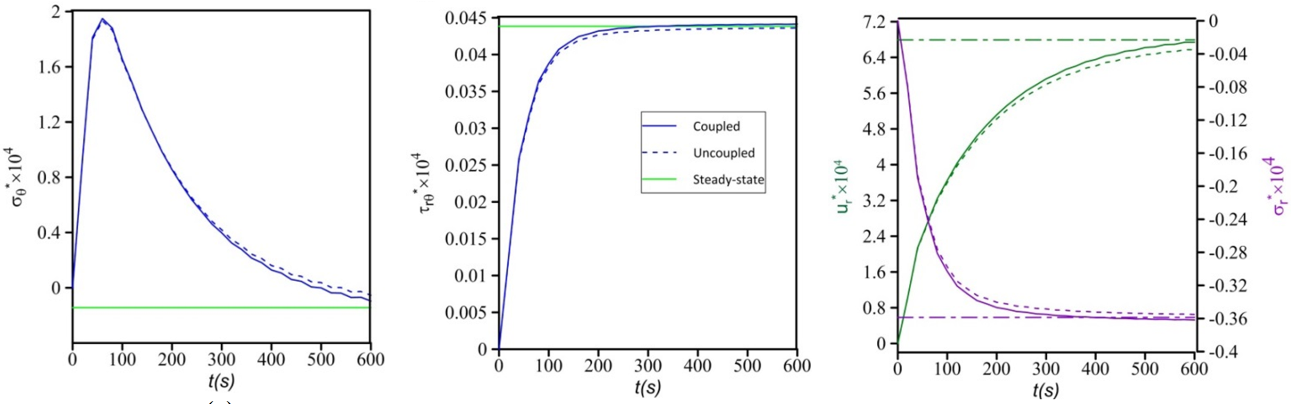


(a) (b) (c)

**Fig. 5.** Distribution of a) Hoop, b) Shear stresses, c) Radial stress along the time, $\beta = 0.5$.

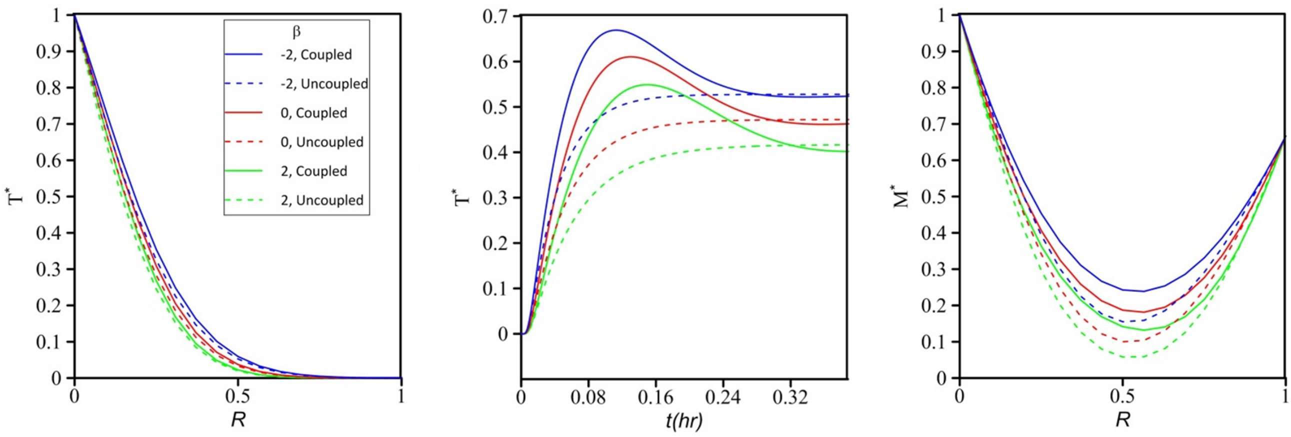


(a) (b) (c)

**Fig. 6.** Effect of inhomogeneity index on the distribution of a) Temperature along radius ($t = 15$s), b) Temperature along time, and c) Moisture along radius ($t = 225$min).

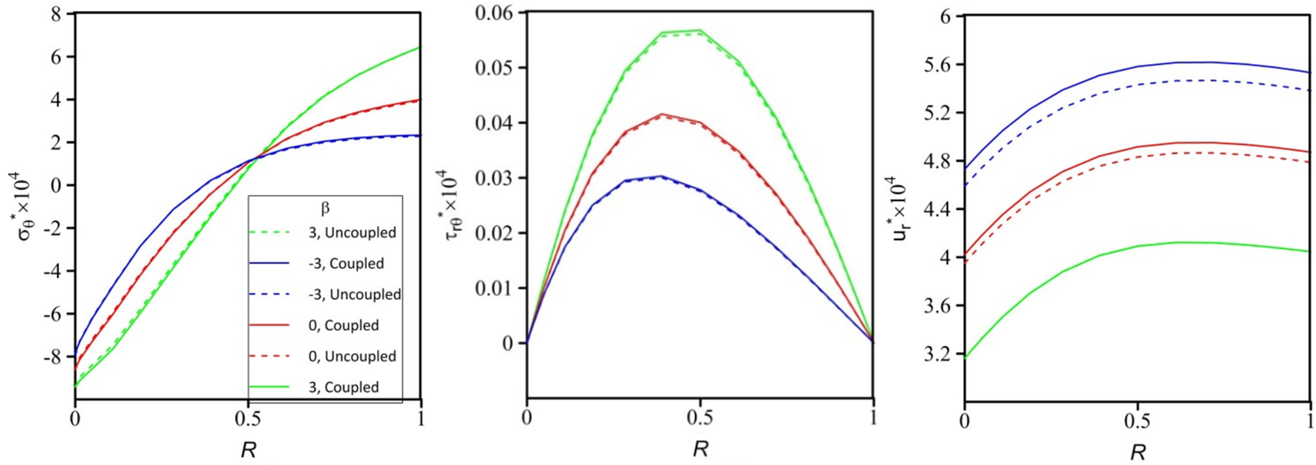


(a) (b) (c)

**Fig. 7.** Effect of inhomogeneity index on the distribution of a) Hoop stress, b) Shear stress, and c) Radial displacement, $t = 200$s.

The effect of coupled hygrothermal loading was investigated for the next case. For this case, it was assumed that $M_a = T_a/10000$. According to Fig. 8, a rise in hygrothermal loading results in a rise in radial displacement, the maximum value of shear stress, and maximum tensile hoop stress at the outer radius. According to the hoop stress distribution, higher hygrothermal loading results in higher tensile stress at the outer radius and higher compressive stress at the inner radius. A similar trend was reported for functionally graded piezomagnetic cylinders under the steady-state hygrothermal loads by Gharibavi and Yi [43]. The high tensile circumferential stress at the exterior radius should be avoided because it can result in growing cracks. In addition, graphs show a point near the middle of thickness in which the circumferential stress is independent of hygrothermal loading.

### *4.3. Dynamic Mechanical Loading*

In this part, the behavior of the FGM cylinder is considered under dynamic internal pressure and the hygrothermal loading is omitted in this case. Hence, there is: $k_L = 0$, $C_d = 0$, $P_a = 10\sin(wt)$MPa, $T_a = T_b = 0$, $M_a = M_b = 0$. To evaluate the influence of frequency of the harmonic excitation on the resulting dynamic responses, variation of the radial displacement of the center point of the cylinder with time is shown in Fig. 9. Fig. 9a shows the case that the excitation frequency is equal to the natural frequency. As expected, the oscillation becomes unbounded. In other cases, the effects of the higher natural modes are detectable. Then, to evaluate the transient behavior of the FGM cylinder, the internal pressure function is considered as:

$$P_a = \begin{cases} 10\sin(wt)\text{MPa} & t < 50\Delta t \\ 0 & t > 50\Delta t \end{cases} \tag{39}$$

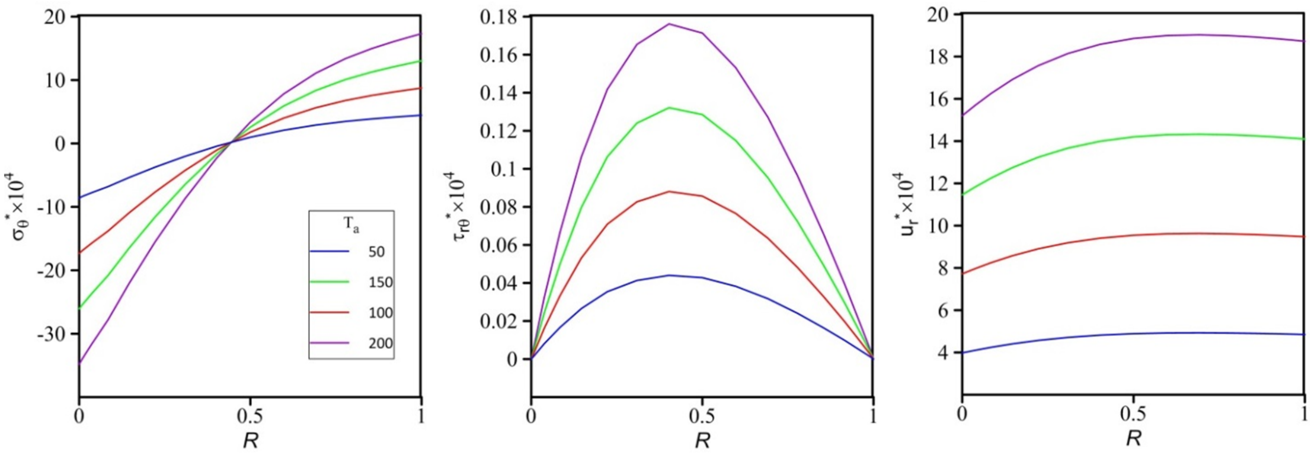


(a) (b) (c)

**Fig. 8.** Effect of coupled hygrothermal loading on the distribution of a) Hoop stress, b) Shear stress, and c) Radial displacement, $\beta = 0.5$, $t = 200$s.

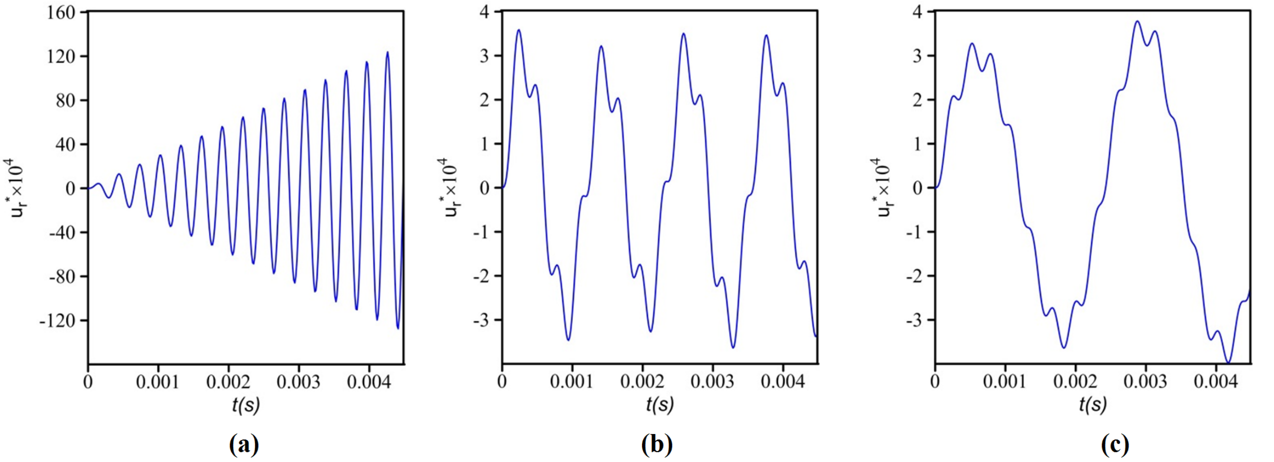


**Fig. 9.** Effect of excitation frequency on the radial displacement a) $w_1 = 21375$, b) $w = 0.25w_1$, and c) $w = 0.125w_1$.

For the first case, the effect of the grading index is investigated on the transient radial displacement. In this case, there is: $k_L = 1 \times 10^{10}$, $C_d = 5 \times 10^5$ and other parameters are as before. As shown in Fig. 10, the negative grading index first increases the oscillation range and then it results in more effect of damping. Conversely, using positive grading index yields first a reduction in oscillation range and then a reduction in the effect of damping.

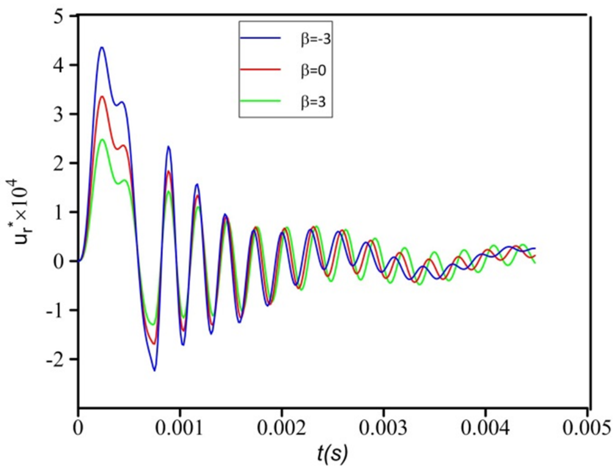


**Fig. 10.** Effect of grading index on the transient radial displacement.

The steady-state hygrothermal loading is the next parameter that was investigated. The used parameters are as previous. According to Fig. 11, a higher hygrothermal boundary condition shifts the graphs up and increases the oscillation range.

The effect of the damping constant was investigated for the last case. The hygrothermal loading is omitted and other parameters are as before. Fig. 12 shows the radial displacement variations. As expected, a higher damping constant of foundation results in more reduction in oscillation range by serving the time and. A similar trend for the effect of the damping constant on the reduction of oscillation range was reported in the literature [44]. Also, Zenkour and Arefi reported a similar influence for the damping constant in functionally graded plates [45].

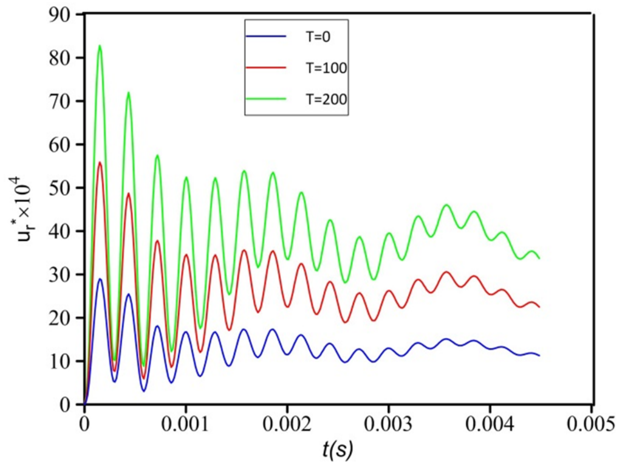


**Fig. 11.** Effect of steady-state hygrothermal loading on the transient radial displacement, $\beta = 0.5$.

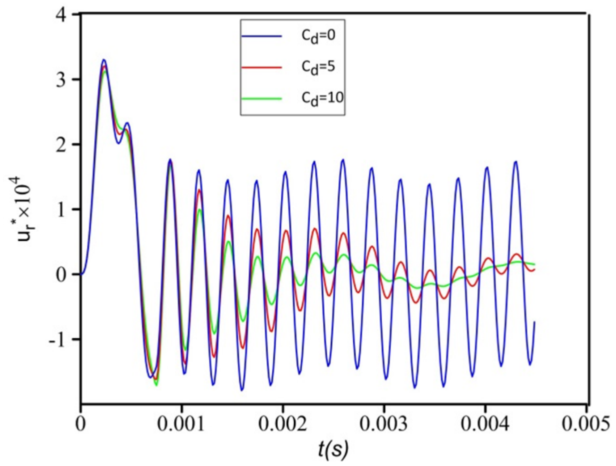


**Fig. 12.** Effect of damping parameter on the transient radial displacement.

## 5. Conclusions

The transient coupled hygrothermal loading was considered for a finite-length FGM cylinder. The material constant of the cylinder was considered as a power-law function. The coupled equations of heat and moisture transfer together with equations were solved employing Fourier series expansion in the longitudinal direction, DQM through the thickness, and the Newmark method in the time domain. The following conclusion can be expressed from the analysis:

1. The results show that the FGM cylinder touches the temperature balance before using the uncoupled model rather than the coupled model. Before reaching the balance, the temperature under the uncoupled model is lower than that of the coupled model. The difference between the coupled model with the uncoupled model is more obvious in moisture rather than temperature.

2. By serving the time, the radial displacement, and maximum hoop stress increase and longitudinal displacement decreases to reach steady-state condition.

3. The negative grading index increases the temperature, moisture, shear stress, and the maximum hoop stress; meanwhile, the influence of the negative grading index is vice versa.

4. The negative grading index first increases the oscillation range and then it results in more effect of damping; meanwhile, the positive grading index has an opposite effect.

## References

[1] M. Saadatfar, M.H. Zarandi, Deformations and stresses of an exponentially graded magneto-electro-elastic non-uniform thickness annular plate which rotates with variable angular speed, Int. J. Appl. Mech., 12(5) (2020) 2050050.

[2] M. Saadatfar, M.H. Zarandi, Effect of angular acceleration on the mechanical behavior of an exponentially graded piezoelectric rotating annular plate with variable thickness, Mech. Based Des. Struct. Mach., (2020). DOI:10.1080/15397734.2020.1751198.

[3] M. Saadatfar, M.H. Zarandi, M. Babaelahi, Effects of porosity, profile of thickness, and angular acceleration on the magneto-electro-elastic behavior of a porous FGMEE rotating disc placed in a constant magnetic field, Proceedings of the Institution of Mechanical Engineers, Proc. Inst. Mech. Eng., Part C, 235(7) (2020) 1241-1257.

[4] M. Shaban, H. Mazaheri, Size-dependent electrostatic analysis of smart micro-sandwich panels with functionally graded core, Acta Mech., 232(1) (2021) 111-133.

[5] M. Shaban, H. Mazaheri, Bending analysis of five-layer curved functionally graded sandwich panel in magnetic field: Closed-form solution, Appl. Math. Mech., 42(2) (2021) 251-274.

[6] M. Jabbari, S. Sohrabpour, M.R. Eslami, General solution for mechanical and thermal stresses in a functionally graded hollow cylinder due to non-axisymmetric steady-state loads, J. Appl. Mech., 70(1) (2003) 111-118.

[7] M. Jabbari, A.H. Mohazzab, A. Bahtui, M.R. Eslami, Analytical solution for three-dimensional stresses in a short length FGM hollow cylinder, Appl. Math. Mech, 87(6) (2007) 413-429.

[8] Y. Ootao, Y. Tanigawa, Transient thermoelastic problem of a functionally graded hollow cylinder due to asymmetrical surface heating, J. Therm. Stresses, 32(12) (2009) 1217-1234.

[9] M. Asgari, M. Akhlaghi, Transient heat conduction in two-dimensional functionally graded hollow cylinder with finite length, Heat Mass Transf., 45(11) (2009) 1383-1392.

[10] A. Loghman, A. Ghorbanpour Arani, S. Amir, A. Vajedi, Magnetothermoelastic creep analysis of functionally graded cylinders, Int. J. Press. Vessel. Pip., 87(7) (2010) 389-395.

[11] H.L. Dai, and Y.N. Rao, Vibration and transient response of a FGM hollow cylinder, Adv. Mater. Struct., 21(6) (2014) 468-476.

[12] M. Zamani Nejad, M. Davoudi Kashkoli, Time-dependent thermo-creep analysis of rotating FGM thick-walled cylindrical pressure vessels under heat flux, Int. J. Eng. Sci., 82 (2014) 222-237.

[13] M. Jabbari, M. Zamani Nejad, M. Ghannad, Thermo-elastic analysis of axially functionally graded rotating thick cylindrical pressure vessels with variable thickness under mechanical loading, Int. J. Eng. Sci., 96 (2015) 1-18.

[14] M. Davoudi Kashkoli, K. Naderan Tahan, M. Zamani Nejad, Time-dependent thermomechanical creep behavior of FGM thick hollow cylindrical shells under non-uniform internal pressure, Int. J. Appl. Mech., 9(6) (2017) 1750086.

[15] A. Najibi, R. Talebitooti, Nonlinear transient thermo-elastic analysis of a 2D-FGM thick hollow finite length cylinder, Compos. B. Eng., 111 (2017) 211-227.

[16] A. Najibi, Mechanical stress reduction in a pressurized 2D-FGM thick hollow cylinder with finite length, Int. J. Press. Vessel. Pip., 153 (2017) 32-44.

[17] A. Hajisadeghian, A. Masoumi, A. Parvizi, Investigating the magnetic field effects on thermomechanical stress behavior of thick-walled cylinder with inner FGM layer, J. Therm. Stresses, 41(3) (2018) 286-301.

[18] M. Saadatfar, Analytical solution for the creep problem of a rotating functionally graded magneto-electro-elastic hollow cylinder in thermal environment, Int. J. Appl. Mech., 11(06) (2019) 1950053.

[19] D. Yarımpabuç, Transient-thermoelastic analysis of periodically rotated functionally graded hollow cylinder, J. Eng. Math., 128(1) (2021) 18.

[20] M. Jabbari, M. Zamani Nejad, Mechanical and thermal stresses in radially functionally graded hollow cylinders with variable thickness due to symmetric loads, Aust. J. Mech. Eng., 18(sup1) (2020) S108-S121.

[21] A.H. Akbarzadeh, Z.T. Chen, Hygrothermal stresses in one-dimensional functionally graded piezoelectric media in constant magnetic field, Compos. Struct., 97 (2013) 317-331.

[22] M.N.M. Allam, A.M. Zenkour, R. Tantawy, Analysis of functionally graded piezoelectric cylinders in a hygrothermal environment, Adv. Appl. Math. Mech., 6(2) (2014) 233-246.

[23] M. Saadatfar, M. Aghaie-Khafri, Hygrothermomagnetoelectroelastic analysis of a functionally graded magnetoelectroelastic hollow sphere resting on an elastic foundation, Smart Mater. Struct., 23(3) (2014) 035004.

[24] M. Saadatfar, M. Aghaie-Khafri, Hygrothermal analysis of a rotating smart exponentially graded cylindrical shell with imperfect bonding supported by an elastic foundation, Aerosp. Sci. Technol., 43 (2015) 37-50.

[25] M. Saadatfar, M. Aghaie-Khafri, On the behavior of a rotating functionally graded hybrid cylindrical shell with imperfect bonding subjected to hygrothermal condition, J. Therm. Stresses, 38(8) (2015) 854-881.

[26] M. Saadatfar, Effect of multiphysics conditions on the behavior of an exponentially graded smart cylindrical shell with imperfect bonding, Meccanica, 50(8) (2015) 2135-2152.

[27] M. Saadatfar, Effect of interlaminar weak bonding and constant magnetic field on the hygrothermal stresses of a FG Hybrid cylindrical shell using DQM, J. Stress Anal., 3(1) (2018) 93-110.

[28] M. Saadatfar, Multiphysical time-dependent creep response of FGMEE hollow cylinder in thermal and humid environment, Mech. Time Depend. Mater., 25(2) (2021) 151-173.

[29] M. Saadatfar, Stress redistribution analysis of piezomagnetic rotating thick-walled cylinder with temperature-and moisture-dependent material properties, J. Appl. Comput. Mech., 6(1) (2020) 90-104.

[30] M. Saadatfar, Transient solution of heat and moisture transfer in a functionally graded hollow cylinder with finite length, Mech. Adv. Compos. Struct., Accepted for publication, (2022), DOI:10.22075/MACS.2022.24225.1355.

[31] M. Saadatfar, Transient response of a hollow functionally graded piezoelectric cylinder subjected to coupled hygrothermal loading, Int. J. Appl. Mech., Accepted for publication, (2021), DOI:10.1142/S175882512150109X.

[32] Y.C. Yang, S.S. Chu, H.L. Lee, S.L. Lin, Hybrid numerical method applied to transient hygrothermal analysis in an annular cylinder, Int. Commun. Heat Mass Transf., 33(1) (2006) 102-111.

[33] H.L. Dai, Z.Q. Zheng, T. Dai, Investigation on a rotating FGPM circular disk under a coupled hygrothermal field, Appl. Math. Model., 46 (2017) 28-47.

[34] T. Dai, Y. Yang, H.L. Dai, H. Tang, Z.Y. Lin, Hygrothermal mechanical behaviors of a porous FG-CRC annular plate with variable thickness considering aggregation of CNTs, Compos. Struct., 215 (2019) 198-213.

[35] Y. Peng, X.Y. Zhang, Y.J. Xie, X.F. Li, Transient hygrothermoelastic response in a cylinder considering non-Fourier hyperbolic heat-moisture coupling, Int. J. Heat Mass Transf., 126 (2018) 1094-1103.

[36] Y. Peng, X.Y. Zhang, X.F. Li, Transient hygrothermoelastic response in a porous cylinder subjected to ramp-type heat-moisture loading, J. Therm. Stresses, 42(12) (2019) 1499-1514.

[37] S.M. Kamal, U.S. Dixit, A. Roy, Q. Liu, V.V. Silberschmidt, Comparison of plane-stress, generalized-plane-strain and 3D FEM elastic–plastic analyses of thick-walled cylinders subjected to radial thermal gradient, Int. J. Mech. Sci., 131-132 (2017) 744-752.

[38] M. Qin, A. Aït-Mokhtar, R. Belarbi, Two-dimensional hygrothermal transfer in porous building materials, Appl. Therm. Eng., 30(16) (2010) 2555-2562.

[39] Y. Rahmati Nezhad, K. Asemi, M. Akhlaghi, Transient solution of temperature field in functionally graded hollow cylinder with finite length using multi layered approach, Int. J. Mech. Mater. Des., 7(1) (2011) 71-82.

[40] J. Eskandari Jam, Y. Rahmati Nezhad, Semi-analytical solution of functionally graded circular short hollow cylinder subject to transient thermal loading, Archive of Mechanical Engineering, 61(3) (2014) 409-432.

[41] A. Bakhshizadeh, M. Zamani Nejad, M. Davoudi Kashkoli, Time-dependent hygro-thermal creep analysis of pressurized FGM rotating thick cylindrical shells subjected to uniform magnetic field, J. Solid Mech., 9(3) (2017) 663-679.

[42] N. Habibi, S. Samawati, O. Ahmadi, Transient thermal stresses analysis in a FPGM cylinder, Mech. Adv. Compos. Struct., 6(2) (2019) 81-94.

[43] M. Gharibavi, J. Yi, Effect of hygro-thermal loading on the two-dimensional response of a functionally graded piezomagnetic cylinder under asymmetric loads, Scientia Iranica, 27(4) (2020) 1916-1932.

[44] M.H. Jalaei, A. Ghorbanpour Arani, Size-dependent static and dynamic responses of embedded double-layered graphene sheets under longitudinal magnetic field with arbitrary boundary conditions, Compos. B. Eng., 142 (2018) 117-130.

[45] A.M. Zenkour, M. Arefi, Nonlocal transient electrothermomechanical vibration and bending analysis of a functionally graded piezoelectric single-layered nanosheet rest on visco-Pasternak foundation, J. Therm. Stresses, 40(2) (2017) 167-184.